Low-frequency fluctuations in vertical cavity lasers: Experiments versus Lang-Kobayashi dynamics

Alessandro Torcini,[1,4] Stephane Barland,[2] Giovanni Giacomelli,[1] and Francesco Marin[3,4]
[1]*Istituto dei Sistemi Complessi, CNR, via Madonna del Piano 10, 50019 Sesto Fiorentino, Italy*
[2]*Institut Non Linéaire de Nice Sophia Antipolis and UMR 6618 CNRS, 1361, route des Lucioles, 06560 Valbonne, France*
[3]*Dipartimento di Fisica, Università di Firenze, and LENS, via Sansone 1, 50019 Sesto Fiorentino, Italy*
[4]*Istituto Nazionale di Fisica Nucleare, Sezione di Firenze, via Sansone 1, 50019 Sesto Fiorentino, Italy*
(Received 3 August 2006; published 1 December 2006)

The limits of applicability of the Lang-Kobayashi (LK) model for a semiconductor laser with optical feedback are analyzed. The model equations, equipped with realistic values of the parameters, are investigated below the solitary laser threshold where low-frequency fluctuations (LFF's) are usually observed. The numerical findings are compared with experimental data obtained for the selected polarization mode from a vertical cavity surface emitting laser (VCSEL) subject to polarization selective external feedback. The comparison reveals the bounds within which the dynamics of the LK model can be considered as realistic. In particular, it clearly demonstrates that the deterministic LK model, for realistic values of the linewidth enhancement factor α, reproduces the LFF's only as a transient dynamics towards one of the stationary modes with maximal gain. A reasonable reproduction of real data from VCSEL's can be obtained only by considering the noisy LK or alternatively deterministic LK model for extremely high α values.

DOI: 10.1103/PhysRevA.74.063801 PACS number(s): 42.65.Sf, 42.55.Px, 05.45.−a, 42.60.Mi

I. INTRODUCTION

The dynamics of semiconductor lasers with optical feedback has been studied both experimentally and theoretically for almost 30 years ([1]; for a review, see, e.g., [2]). The interest in such a configuration, commonly encountered in many applications (e.g., communication in optical fibers, optical data storage, sensing, etc.) arises from the rich phenomenology observed, ranging from multistability, bursting, intermittency, and irregular and rare drops of the intensity [low-frequency fluctuations (LFF's)] and transition to developed chaos [coherence collapse (CC)]. A complete understanding of the physical mechanisms as the basis of such complex behavior is, however, still lacking. In particular, the origin of the LFF regime has been under debate since the very first observations and yet this puzzling problem has not been solved. Their origin was ascribed to stochastic effects [3,4] or to deterministic but chaotic dynamics [5] and, more recently, even to the interplay between regular periodic and quasiperiodic solutions [6]. The LFF dynamics has been investigated by using several types of emitters, mainly edge-emitting: ranging from longitudinal multimode [7–13] to single-mode distributed-feedback (DFB) [14] semiconductor lasers.

From the experimental point of view, a complete characterization of the LFF dynamics is quite difficult, because of the very different time scales involved [15]. Indeed, fast oscillations on the 10-ps range have been observed with streak camera measurements [16,17], representing the fundamental scale on which the system evolves. On the other hand, the duration of such a fast-pulsing regime between LFF events can be as long as hundreds of nanoseconds or even microseconds. In the literature, the LFF dynamics has been experimentally characterized in several manners, starting from a relatively simple statistical analysis of the time separation T between LFF's [14,18,19] (relating the average $\langle T \rangle$ between LFF's with the pump current) to Hurst exponents for the laser phase dynamics [20].

A widely used theoretical description of the system is the Lang-Kobayashi (LK) model [21], introduced in 1980 in an effort to provide a simplified but effective analysis of an edge-emitting semiconductor laser optically coupled with a distant reflector. In the model, both multiple reflections from the mirror (low coupling) and possible multimodal structure of the laser were neglected. The opportunity to include such effects has been discussed in several papers [7–9,12,22,23], but the model continues to be presented as the standard theoretical approach to the system. While most of the phenomenology observed in the different experiments is represented by the model, quite often a more precise or quantitative comparison is obtained at the expense of a choice of parameters far from those actually measured or even physically plausible.

Recently, a configuration has been proposed and studied based on a vertical cavity surface emitting laser (VCSEL) with a polarized optical feedback [15]. Such a laser is longitudinal single-mode (due to the very short cavity) but may support different, high-order transverse modes for strong enough pumping current (see, e.g., [24]). The symmetry of the cavity allows also for possible laser action on two different, linear polarizations selected by the crystal axis. The dynamics of the VCSEL with isotropic optical feedback has been examined experimentally in [23,25] and theoretically in [26], while the role played by polarized optical feedback has been discussed in [27–29]. In particular, the setup used in [15] employed a polarizer in the feedback arm, in order to couple back only the radiation of one polarization; moreover, a suitable range of pump current was chosen, to assure single transverse mode behavior. In such a configuration, the appearance of LFF's was reported and characterized. The possibility to control the role of the laser modes in the dynamics in this setup allows for a consistent description via the LK

model and therefore for an effective test of its predictions, at variance with a similar setup where instead polarization selection was not used [23,25].

Our aim in the present paper is to clarify the origin of the LFF dynamics by comparing the experimental measurements done on a VCSEL with numerical results obtained by integrating the LK equations with parameter values obtained from analysis of the same VCSEL sample [32]. In particular, this comparison suggests that the experimental data can be better reproduced by a stochastic version of the LK equation, since the evolution of the deterministic LK model usually ends up in a stable lasing state, in agreement with the results reported in [14]. Moreover, our analysis supports the idea that the LFF phenomenon can be interpreted as a biased diffusive motion towards a threshold in the presence of a reset mechanism.

In Sec. II we describe our experimental setup, reporting the main phenomenology observed in the range of variation of the more relevant parameters of the system: namely, the pump current and the phase of the feedback. The LK model is introduced and commented on in Sec. III, together with the numerical methods employed for its integration and the choice of parameter values derived from the experiment. In Sec. IV the properties of the stationary solutions are discussed, while in Sec. V a careful characterization of the deterministic model is given, detailing the transient phenomena and the Lyapunov analysis. In Sec. VI the effect of noise is introduced and analyzed, discussing also its possible importance in the experiment. A detailed comparison of the numerical results with the experimental measurements is given in Sec. VII, with particular regard to the distribution of the intensity and interevent times for different parameter choices, including the α factor and the acquisition bandwidths. Finally, we draw our conclusions in Sec. VIII.

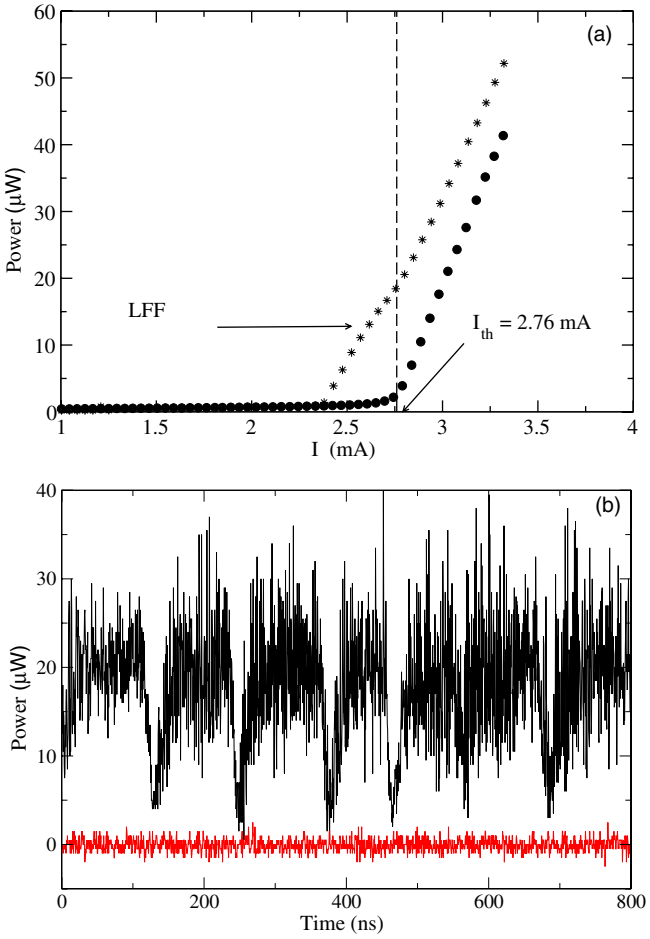

FIG. 1. (Color online) (a) Average power output versus the input current for the solitary laser (dots) and for the laser with feedback (stars). (b) Polarization modes: power outputs as a function of time for the VCSEL with feedback at I=2.64 mA. Upper trace (black): main polarization. Lower trace (red): secondary polarization.

II. EXPERIMENTAL SETUP AND SETTINGS

The experimental measurements are performed using a VCSEL semiconductor laser with moderate polarized optical feedback. In particular, our analysis is limited to a regime of pumping below the solitary threshold $I_{th} \sim 2.76$ mA, where the VCSEL emits light in a single linearly polarized transverse mode. Longitudinal modes are not allowed by the cavity, and other transverse modes are not present up to currents ~6.5 mA. The solitary laser emission remains well polarized up to roughly the same current [see Fig. 1(b)].

The technical details of the source are the following. The laser is an air-post VCSEL made by the Swiss Center for Electronics and Nanotechnology (CSEM) [30], operating around 770 nm. The mesa diameter is 9.4 μm, a ring contact defines the output window with a diameter of 5 μm, and the active medium is composed of three 8-nm quantum wells. The temperature of the laser case is stabilized within 1 mK, the pump current is controlled by a homemade battery-operated power supply whose current noise is below 40 pA/Hz$^{-1/2}$ in the frequency range from 1 kHz to 3 MHz.

The feedback is applied to the polarization direction of the solitary laser emission. The external cavity includes collimation optics, two polarizers, a variable attenuator, and feedback mirrors that are mounted on a piezoelectric transducer at about 50 cm from the laser. The output radiation, after optical isolators, is detected by an avalanche photodiode with a bandwidth of about 2 GHz, whose signal, sometimes after low-pass filtering, is recorded by a 4-GHz bandwidth digital scope. More details on the experiment can be found in Refs. [15,31].

Optical feedback results in a reduced threshold I_{th}^{red} ~2.42 mA, as shown in Fig. 1(a). We have examined the dynamic behavior of the output intensity for various pump currents, both above and below I_{th}, with particular attention paid to possible effects of the feedback phase $\Delta\phi$ which is varied by acting on the external mirror piezoelectric transducer.

As shown in Fig. 2, we can identify several regimes: (I) at $I < I_{th}$ one observes a single-mode LFF dynamics [i.e., the main polarization exhibits LFF's, while the secondary polarization remains off; see Fig. 1(b)]. (II) $I_{th} < I < 3.5$ mA: in this regime the LFF dynamics of the main polarization is accompanied by a synchronized spiking behavior in the secondary polarization (coupled-mode LFF's). This regime was analyzed in Ref. [15] and, in more details, in Ref. [31],

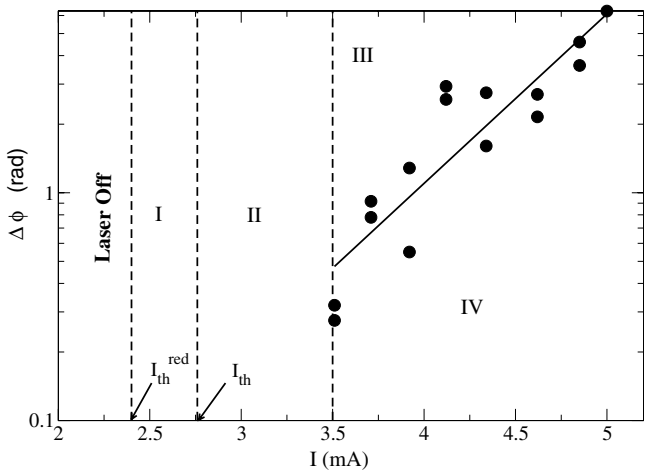

FIG. 2. Phase diagram of the VCSEL with feedback: phase of the feedback $\Delta\phi$ as a function of the pump current I. The roman numbers denote regions of different dynamical regimes: (I) single-mode LFF, (II) two-mode LFF, (III) coherence collapse, and (IV) stable emission. The vertical dashed line indicates (from low to high current) successive current thresholds: the reduced one I_{th}^{red}, the solitary laser one I_{th}, and the current value separating LFF's from coherence collapse. The dots represent the maximal $\Delta\phi$ for which the laser emission remains stable, while the solid line is a guide for eyes to distinguish regions III from IV.

where it is proposed that the dynamics of the secondary polarization is driven by the main polarization, whose behavior is not influenced by the orthogonal polarization mode. For larger pump current one begins to observe coherence collapse [regime (III) in Fig. 2] and moreover the feedback phase begins to play a fundamental role. In particular, for increasing I in larger and larger portions of the phase interval the laser is stationary [regime (IV) in Fig. 2]. This phenomenon is not yet understood, the and it will be the subject of a future analysis [27].

Anyway, in the present paper we will limit our analysis to regime (I) (i.e., for $I<I_{th}$), where the VCSEL has a single-mode LFF dynamics and the phase delay of the feedback does not play any role. We remark that this statement is suggested by the experiment, where the phase stability would be enough to discriminate such effects, as shown in the analysis of regimes III and IV.

III. NUMERICAL MODEL AND METHODS

The dynamics of the VCSEL for $I<I_{th}$ is a purely single-mode dynamics, and therefore we expect that it could be reproduced by employing the LK [21] rate equations for the complex field $E(t)=\rho(t)\exp i\psi(t)$ and the carrier density $n(t)$. In order to achieve an accurate and reliable comparison of the numerical results with the experimental ones we will employ for our simulations the laser working parameters reported in Table I. These parameters have been determined via a series of suitable experiments for exactly the same VCSEL employed to obtain the measurements examined in this paper [32]. The only parameter lacking that was not possible to obtain in the previous characterization is the feedback strength, which is, however, determined from the threshold reduction.

TABLE I. Experimental values of the parameters entering in the model (1) (from [32]).

Description	Symbol	Value
Linewidth enhancement factor	α	3.2 ± 0.1
Photon lifetime in the cavity	τ_p	12 ± 1 ps
Carrier lifetime	τ_n	0.37 ± 0.02 ns
External round-trip time	τ	3.63 ns
Variance of the spontaneous emission noise	R_{sp}	$(2.3\pm0.6)\times10^{-4}$ ps^{-1}
Reduced gain	η	5.8 ± 0.6

In this article we use the rate equations derived in Ref. [32] for the single-mode solitary laser, modified to include the feedback. Defining the deviation Δn of the carrier density from transparency normalized to have a unitary value at threshold—i.e., $\Delta n=(n-1)/(n_{th}-1)$—the following form is obtained [32]:

$$\tau_n\dot{\Delta n} = -\Delta n + 1 + \eta(\mu-1) - \Delta n|E|^2,$$

$$\dot{E} = \frac{1+i\alpha}{2\tau_p}[\Delta n - 1]E + \frac{k}{\tau_p}e^{-i\omega\tau}E(t-\tau) + \sqrt{R_0}\tilde{\xi}(t), \quad (1)$$

where $\tilde{\xi}(t)=\xi_R(t)+i\xi_I(t)$ is a complex Gaussian noise term with zero mean and correlation given by $\langle\xi_R(t)\xi_R(0)\rangle=\langle\xi_I(t)\xi_I(0)\rangle=\delta(t)$ and $\langle\xi_R(t)\xi_I(0)\rangle=0$. The noise variance $R_0=(n/n_{th})^2R_{sp}$ represents a multiplicative noise term proportional to the square of the reduced carrier density n/n_{th} (n_{th} being the threshold carrier density) and to the variance of the spontaneous emission noise R_{sp}. The parameter $\mu=I/I_{th}$ is the pump current rescaled to unity at threshold, τ_n and τ_p are carrier and photon lifetimes, respectively, τ is the delay (or external round trip time), α is the linewidth enhancement factor, and η is the reduced gain [for the exact definitions of these quantities in terms of the laser parameters and for the approximations employed to derive (1) see Ref. [32]].

By reexpressing the time scale in terms of the photon lifetime (τ_p) the equations assume the usual form for the LK model and read as

$$T\dot{\Delta n} = -\Delta n + p - \Delta n|E|^2,$$

$$\dot{E} = \frac{1+i\alpha}{2}[\Delta n - 1]E + k\,e^{-i\phi}E(t-\tau) + \sqrt{R}\tilde{\xi}(t), \quad (2)$$

where $T=\tau_n/\tau_p$, $p=1+\eta(\mu-1)$, $R=(n/n_{th})^2R_{sp}\tau_p$, and $\phi=\omega\tau$. Moreover, by assuming that $n\sim n_{th}$ the noise terms become additive with an adimensional variance $R=2.76\times10^{-3}$, the other quantities entering in (2), expressed in τ_p units, are $\tau=302.5$, $\phi=8.743\times10^6$, and $T=30.8333$, the numerical values having been obtained by employing the parameter values in Table I.

In order to reproduce the power-current response curve for two different experimental data sets we have chosen

feedback strengths $k=0.25$ and 0.35, while typically we considered pump currents and linewidth enhancement factors in the ranges $0.9 \leqslant \mu \leqslant 1.20$ and $3 \leqslant \alpha \leqslant 5$, respectively.

The deterministic equations (2) with $R \equiv 0$ have been integrated by employing the method introduced by Farmer in 1982 [33] equipped with a standard fourth-order Runge-Kutta scheme, while for integrating the equations with the stochastic terms we have employed a Heun integration scheme [34]. The simulations have been performed by integrating the field variables with time steps of duration $\Delta t = \tau/(N-1)$, with $N=1000-10\,000$.

The dynamical properties of the system can be estimated in terms of the associated Lyapunov spectrum, which fully characterizes the linear instabilities of infinitesimal perturbations of the reference system. By following the approach reported in [33], we have estimated the Lyapunov spectrum $\{\lambda_k\}$ $(k=1,\ldots,2N+1)$ by integrating the linearized dynamics associated with Eqs. (2) in the tangent space and by performing periodic Gram-Schmidt ortho-normalizations according to the method reported in [35]. The Lyapunov eigenvalues λ_k are real numbers ordered from the largest to the smallest; a positive maximal Lyapunov λ_1 is an indication that the dynamics of the system is chaotic. Moreover, from knowledge of the Lyapunov spectrum it is possible to obtain an estimation of the number of degrees of freedom actively involved in the chaotic dynamics in terms of the Kaplan-Yorke dimension [36] $D_{KY}=j+\Sigma_{k=1}^{j}\lambda_k/|\lambda_{j+1}|$, j being the maximal index for which $\Sigma_{k=1}^{j}\lambda_k \geqslant 0$.

IV. STATIONARY SOLUTIONS

A first characterization of the phase space of the LK system can be achieved by individuating the corresponding stationary solutions and by analyzing their stability properties. The stationary solutions of the above set of equations can be found by setting $\dot{\rho}=\Delta\dot{n}=0$ and $\dot{\psi}=\Omega$—i.e., by looking for solutions of the form

$$E_S(t) = \rho_S\, e^{i\Omega t} \text{ and } \Delta n(t) = \Delta n_S. \tag{3}$$

These solutions are termed external cavity modes (ECM's) and correspond to stationary lasing states. The ECM's, once parametrized in terms of the variable $\theta=\phi+\Omega\tau$, assume the following expressions [37]:

$$X_S = \frac{(\Delta n_S - 1)}{2} = -k\cos(\theta), \quad \rho_S^2 = 2\frac{J - X_S}{2X_S + 1} \geqslant 0, \quad \Omega = \frac{\theta - \phi}{\tau} = -k\sqrt{1+\alpha^2}\,\sin(\theta + \theta_0), \tag{4}$$

where $J=(p-1)/2$, $\theta_0=\arctan(\alpha)$, and $-\pi < \theta \leqslant \pi$.

The stability properties of the ECM's can be obtained by estimating the associated Floquet spectrum $\{\Lambda_n\}$; these eigenvalues are typically complex and their number is infinite, due to the delay term present in the LK equations. However, the stability properties of the ECM's are determined by the eigenvalues with the largest real part, in particular by the maximal one $\Lambda^M=(\mathrm{Re}\,\Lambda^M, \mathrm{Im}\,\Lambda^M)$. These can be easily determined by solving the characteristic equation obtained by linearizing around a certain ECM:

$$\begin{aligned} &Z_n^2[\Lambda_n + \varepsilon(1+\rho_S^2)] + 2Z_n\{\Lambda_n\cos(\theta)[\Lambda_n + \varepsilon(1+\rho_S^2)] \\ &\quad + \varepsilon\rho_S^2(1-2k\cos(\theta))[\cos(\theta) - \alpha\sin(\theta)]/2\} \\ &\quad + \Lambda_n^2[\Lambda_n + \varepsilon(1+\rho_S^2)] + \Lambda_n\varepsilon\rho_S^2(1-2k\cos(\theta)) \\ &\equiv a_n Z_n^2 + 2b_n Z_n + c_n = 0, \end{aligned} \tag{5}$$

where $Z_n=k(1-e^{-\Lambda_n\tau})$ and $\varepsilon=1/T$. The *pseudocontinuous* spectrum [38] can be obtained by solving Eq. (5) in terms of Z_n and by considering Λ_n as a parameter. In this case the solutions of the corresponding second-order equation are

$$\Lambda_n^{\pm} = -\frac{1}{\tau}\ln\left[1 + \frac{b_n \mp \sqrt{b_n^2 - a_n c_n}}{k a_n}\right] + i2\pi n, \tag{6}$$

and by self-consistently solving the above equation one can find all the eigenvalues, which are arranged in two branches. However, the spectrum contains also isolated eigenvalues, which can be obtained by solving directly Eq. (5) in terms of Λ_n and by considering Z_n as a parameter. In this case the equation is cubic and by solving self-consistently its expression one finds (up to) three distinct eigenvalues. While the pseudocontinuous spectrum emerges due to the presence of the delay in the system, the isolated eigenvalues originate from those characterizing the three-dimensional single-laser rate equations in the absence of the delay—i.e., Eq. (2) with $\tau=0$ [38].

Typically, depending on their linear stability properties ECM's are divided into *modes* and *antimodes* [39]. Antimodes are characterized by a positive real eigenvalue and are therefore unstable. For the modes instead the maximal real eigenvalue is zero and they are unstable whenever the associated spectrum crosses the imaginary axis. Various types of instabilities can be observed for these delayed systems, and they can be classified in analogy with spatially extended systems such as, for example, *modulational-type* or *Turing-type* instabilities [37,38]. Examples of the unstable branch for the spectra $\{\Lambda_k\}$ associated with Turing-type and modulational-type instabilities are reported in Fig. 3(a); for a classification of the possible instabilities of equilibria for delay-differential equations, see [38].

In particular, the modes correspond to θ values located within the interval $[\theta_2, \theta_1]$, where $\theta_1 \sim \arctan(1/\alpha)$ and $\theta_2 \sim -\pi + \arctan(1/\alpha)$. Moreover, stationary solutions are acceptable only if they correspond to positive intensities $\rho_S^2 \geqslant 0$—i.e., if they are situated within the interval $[-\theta_R, \theta_R]$ with $\theta_R=\arccos(-J/k)$. In the range of parameters examined in the present paper the number of stable modes (SM's) is always between 2 and 4 and they are located in a narrow interval of θ located around zero [i.e., around the so-called maximum gain mode (MGM)].

As we will report in the following section, by integrating the deterministic version of the model (2) for moderate α and μ values, we always observe a relaxation towards one of the SM's. In particular for $3 < \alpha < 5$ the dynamics seems to relax always towards one of the SM's located in proximity of the MGM (corresponding to $\theta \equiv 0$) [see Fig. 3(b)]. It should be noticed that the MGM is a solution of the system only for appropriate choices of ϕ. An example of typical ECM's is reported in Fig. 3(b) for the present system for $\alpha=5$ and μ

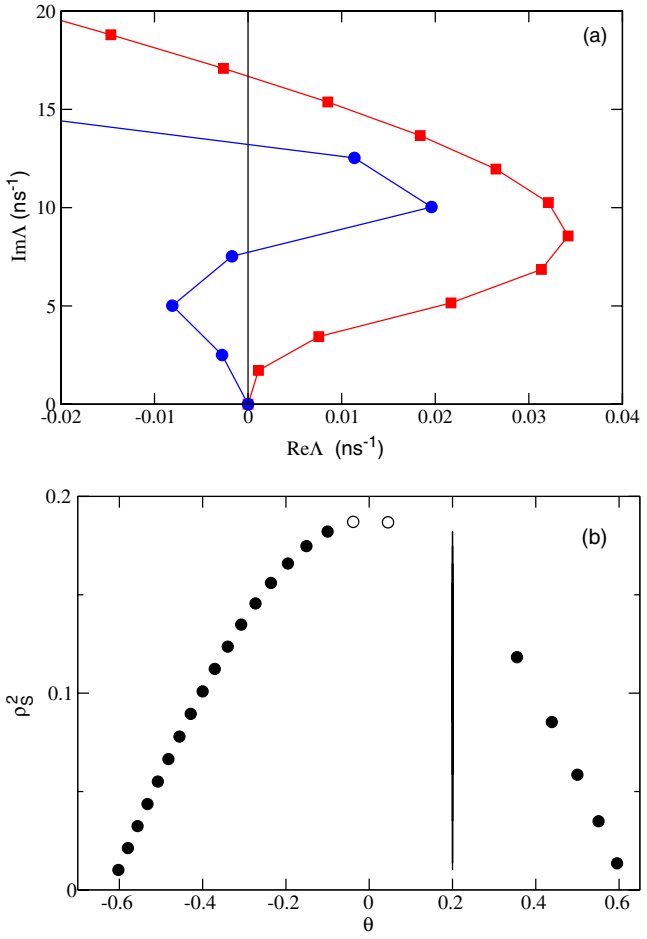

FIG. 3. (Color online) (a) Unstable branch Λ associated with specific modes of the LK model. The mode $\theta=-0.32$ for $\alpha=3.20$ reveals a sort of modulational instability (red squares), while the mode $\theta=-0.08$ for $\alpha=3.22$ shows a Turing-like instability (blue circles). The results refer to $\mu=0.93$. Due to the symmetry of the spectra, only the part corresponding to $\mathrm{Im}\,\Lambda>0$ is displayed. (b) Intensities versus θ for ECM's of Eq. (2) with $\mu=0.93$ and $\alpha=5$. The solid line indicates θ_1. The ECM's with $\theta<\theta_1$ are modes, while the others are antimodes. The open circles indicate the stable modes towards which a relaxation of the system has been observed by considering up to 100 different random initial conditions.

$=0.93$; in this case, two stable attracting modes have been identified. Recently, a similar coexistence of two stable solutions located in the proximity of the MGM has been reported experimentally for an edge-emitter laser with a low level of optical feedback [40].

As reported in [37] the stability properties of the MGM do not depend on α; therefore, it is reasonable to expect that some SM's will be always present in a narrow window around θ for any chosen linewidth enhancement factor [39] and that they will coexist with the chaotic dynamics, as observed experimentally in [41].

V. DETERMINISTIC DYNAMICS

An open problem concerning the deterministic LK equations is if and for which range of parameters these equations faithfully reproduce the experimentally observed dynamics. Particular interest is usually focused on the α value to be employed to obtain a realistic behavior of the model.

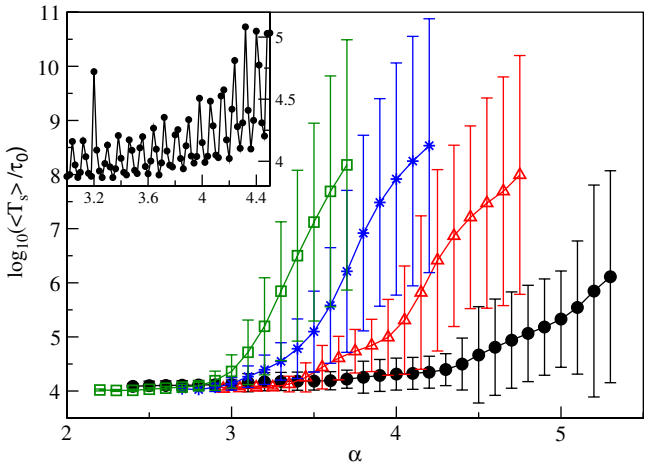

FIG. 4. (Color online) Logarithm of the transient times $\langle T_s\rangle$ as a function of α for various μ values: namely, $\mu=0.93$ (black solid circles), 0.95 (red open triangles), 0.97 (blue asterisks), and 0.99 (green open squares). The data refer to $k=0.25$, $\Gamma=10^{-5}$, $t_w=1000\tau=3.630$ μs, and $M\sim 10-100$, and they have been obtained by employing an integration time step $\Delta t=3.63$ ps. The time scale of the figure is $\tau_0=1$ ns. The bars reported for each measured value indicate the range of variability of $\langle T_s\rangle$ (within an α interval of amplitude 0.1) due to its finer structure shown in the inset. In the inset are displayed the transient times for $\mu=0.93$ reported at a higher resolution in α—namely, for a resolution of 0.02.

A. LFF's as a transient phenomenon

To answer this question we consider the deterministic version of the model (2) (i.e., by assuming $R\equiv 0$) equipped with the parameter values deduced by the experimental data [32] apart for μ and α, which will be varied. In particular, we would like to understand if the system shows a LFF behavior and if such dynamics is statistically stationary or not. In order to verify it, we initialize randomly the amplitude $\rho(t=0)$, the phase $\phi(t=0)$, and the excess carrier density $\Delta n(t=0)$; then, we follow the dynamics and examine the evolution of the field intensity $\rho^2(t)$. If the dynamics end up on a stationary solution, we register the time T_s necessary to reach it and then we average this time over many (M) different initial conditions. In order to measure T_s, we estimate the time needed for the standard deviation of the intensity (evaluated over subwindows of time duration t_w) to decrease below a chosen threshold Γ. The average times $\langle T_s\rangle$ are reported in Fig. 4

The main result shown in Fig. 4 is that the system after a transitory phase (shorter or longer) settles down to a SM and that the duration of the transient increases for increasing α or μ values. Preliminary indications in this direction have been previously reported in [14]. These results clearly indicate that the LFF dynamics is just a transient phenomenon for the deterministic LK equation for commonly employed α values (i.e., for $\alpha\sim 3.0-3.5$). For each fixed μ it seems that $\langle T_s\rangle$

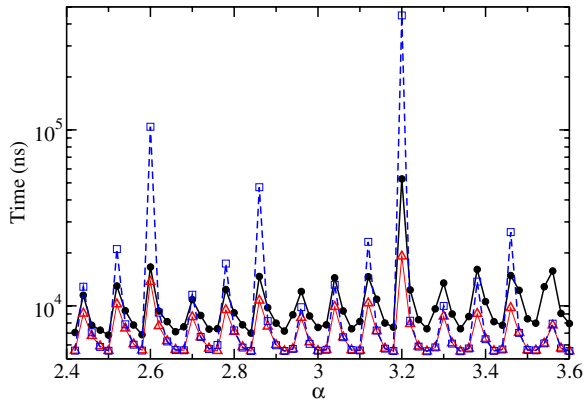

FIG. 5. (Color online) Transient times $\langle T_s \rangle$ (black solid circles), T_{est} (red open triangles), and T_1 (blue open squares) in nanoseconds as a function of α. The results have been obtained by examining the decay of $\rho^2(t)$ with $\Gamma=10^{-5}$ and $t_w=1000\tau=3.630$ μs and $M \sim 100-500$. The integration time step employed is $\Delta t=0.363$ ps and the data refer to $k=0.25$ and $\mu=0.93$.

diverges above some "critical" α value; however, we cannot exclude the possibility that the system will also in this case finally converge to a SM. At least we can consider the reported critical values as lower bounds above which LFF's could occur as a stationary phenomenon and not as a transitory state. With the chosen numerical accuracy and due to the available computational resources, for any practical purpose a transient longer than 0.1–1 s can be considered as an infinite time.

An interesting feature is that the variability of $\langle T_s \rangle$ with α is quite wild and it reflects the stability of the modes in proximity of the MGM, as shown in Fig. 5. However, the average values $\langle T_s \rangle$ (averaged also over α intervals of width 0.1) still indicates a clear trend of the transient times to increase with α.

We expect that the time scale associated with the convergence to a stable mode is ruled by the eigenvalue with the maximal real part (apart from the eigenvalue zero, which is always present due to the phase invariance of the LK equations). In particular we expect that the intensity of the signal will converge towards the stable mode as

$$\rho^2(t) \sim \rho^2(0) e^{2\mathrm{Re}\ \Lambda^M t} \cos(2\mathrm{Im}\ \Lambda^M t) + \rho_S^2,$$

where Λ^M is the eigenvalue with maximal (nonzero) real part associated with the considered stable solution. For small μ we have observed that the dynamics can collapse to different stable solutions (typically, from 1 to 3). By estimating the probability $P_m=N_m/M$ to end up in one of these states (N_m being the number of initial conditions converging to the m mode) and by indicating the corresponding eigenvalue with maximal real part as $\Lambda^M(m)$, a reasonable estimate of $\langle T_s \rangle$ is given by

$$T_{est} = \frac{\ln \Gamma}{2} \sum_m \frac{P_m}{|\mathrm{Re}\ \Lambda^M(m)|}, \tag{7}$$

where Γ is the employed threshold. As can be seen in Fig. 5, the estimation is quite good and the periodicity of the two quantities is identical in the examined range of α values and for $\mu=0.93$. The expression (7) always gives a good estimate of $\langle T_s \rangle$ for $\alpha<4$ and for $\mu<1$, but the agreement worsens for increasing α values.

However, an even more rough estimate is capable of giving a reasonable approximation of $\langle T_s \rangle$ and in particular of capturing its periodicity. This estimate is simply given by

$$T_1 = \frac{\ln \Gamma}{2} \frac{1}{|\mathrm{Re}\ \bar{\Lambda}^M|}, \tag{8}$$

where $\bar{\Lambda}^M$ is the eigenvalue with maximal nonzero real part associated with the stable mode with higher θ (i.e., the first stable mode located in the proximity of the antimode boundary). The agreement between T_1 and $\langle T_s \rangle$ shown in Fig. 5 suggests that the stability properties of this particular SM essentially drive the relaxation dynamics of the system and in particular the peaks in Fig. 5 are related to Hopf bifurcation of this mode (i.e., to the crossing of the antimode boundary θ_1).

From the present analysis it emerges that the stable modes play a relevant role for the (transient) dynamics of the deterministic LK equations at least for $\alpha<4$. Moreover, the observed strongly fluctuating behavior of $\langle T_s \rangle$ as a function of α indicates that the choice of this parameter is quite critical, since a small variation can lead to an increase of an order of magnitude of the transient time [45].

B. Lyapunov analysis

We have characterized the transient dynamics preceding the collapse in the stationary state in terms of the maximal Lyapunov λ_1 and of the associated Kaplan-Yorke (or Lyapunov) dimension D_{KY}. In particular, these quantities, reported in Fig. 6, have been estimated by integrating the linearized dynamics for a sufficiently long time period T_{int} and by averaging over M different initial realizations.

It is clear from the figures that the average maximal Lyapunov exponent $\langle \lambda_1 \rangle$ is definitely not zero for all situations considered and that it increases (almost steadily) with the parameter α as well as with the pump parameter. Moreover, this indicator also reflects the stability properties of the SM's located in proximity of the MGM by exhibiting large oscillations as a function of α, as shown in the inset of Fig. 6(a).

The values of $\langle D_{KY} \rangle$ reported in Fig. 6(b) clearly indicate that the system cannot be described as low dimensional, even during the transient and even below the solitary laser threshold. As a matter of fact the number of active degrees of freedom ranges between 10 and 50. It should be noticed that $\langle D_{KY} \rangle$ is determined by the instability properties not only of antimodes and but also of modes that have bifurcated (via Hopf instabilities), becoming unstable for increasing α.

VI. NOISY DYNAMICS

We have examined the dynamics (1) for increasing level of noise: namely, for $10^{-6}<R<10^{-2}$. Also, in this case, for $\alpha=3.3$ and for noise levels smaller than 10^{-3} the LFF dy-

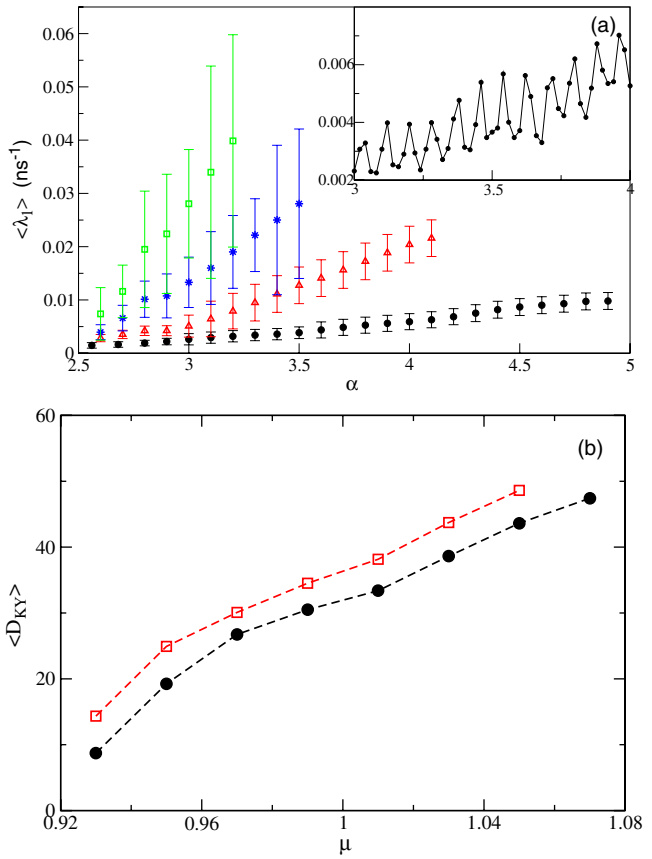

FIG. 6. (Color online) (a) Average maximal Lyapunov exponents $\langle \lambda_1 \rangle$ as a function of α and for various μ values below threshold: namely, $\mu=0.93$ (black solid circles), 0.95 (red open triangles), 0.97 (blue asterisks), and 0.99 (green open squares). The bars reported for each measured value indicate the range of variability of $\langle \lambda_1 \rangle$ due to its finer structure as measured within an α interval of width 0.1. In the inset the data for $\langle \lambda_1 \rangle$ are reported for a higher resolution in α (namely, 0.02) for $\mu=0.93$. (b) Average Kaplan-Yorke dimensions $\langle D_{KY} \rangle$ as a function of μ for $\alpha=4$ (black solid circles) and 5 (red open squares). All the data refer to $k=0.25$, for the $\langle \lambda_1 \rangle$ estimation $\Delta t=0.363$ ps, $M=500$, and $T_{int}=3.63$ ms, while for the $\langle D_{KY} \rangle$ evaluation $\Delta t=3.63$ ps, $M=20$, and $T_{int}=0.14$ ms.

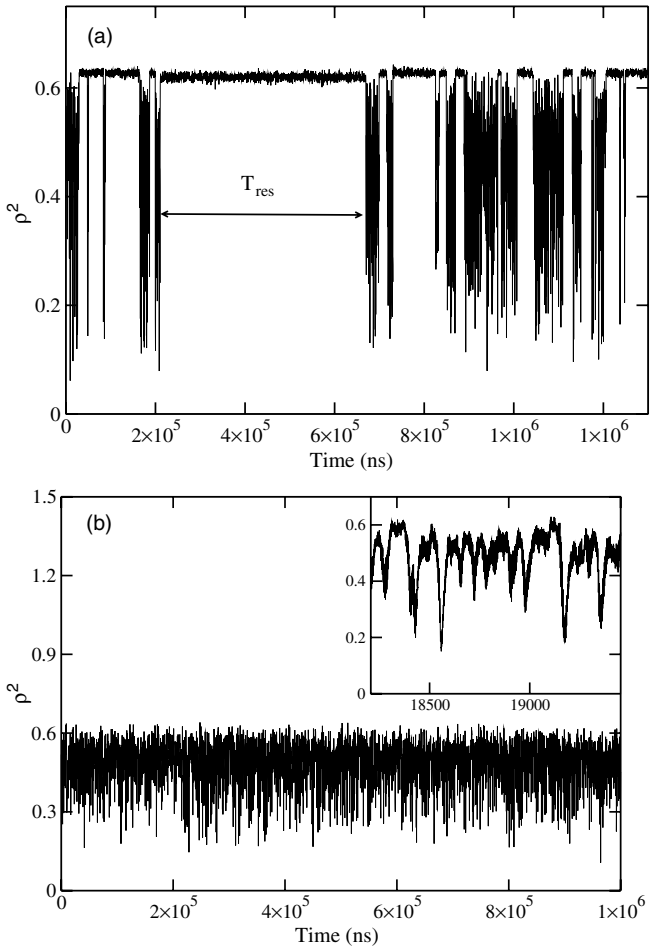

FIG. 7. Intensity of the field ρ^2 as a function of the time for the noisy LK equations. The data have been filtered with a low-pass filter at 80 MHz and refer to $\mu=0.97$ and $\alpha=3.3$. The results reported in (a) correspond to a noise variance $R=3\times10^{-4}$, while those in (b) are relative to $R=3\times10^{-3}$. In (a) a typical time of residence T_{res} around one of the SM's is indicated. The inset in (b) is an enlargement of the actual dynamics.

namics only occurs during a transient. However, for increasing R values we observed a transition to sustained LFF's and the transition region was characterized by an intermittent behavior. These behaviors are exemplified in Fig. 7 for $\alpha=3.3$ and $\mu=0.97$. As shown in Fig. 7(a) the orbit spends long times in proximity of one of the SM's and then, due to noise fluctuations, escapes from the attraction basin associated with the stable solution and exhibits LFF's before being newly reattracted by the SM. This intermittent dynamics can be interpreted as an activated escape process induced by noise fluctuations, and therefore the average residence time $\langle T_{res} \rangle$ in the attraction basin of the SM can be expressed in the following way:

$$\langle T_{res} \rangle \propto \exp[W/R], \tag{9}$$

where W represents a barrier that the orbit should overcome in order to escape from the SM valley. As shown in Fig. 8 the process can be indeed interpreted in terms of the Kramers expression (9) for $2\times10^{-4}<R<7\times10^{-4}$. It means that for $R<W$ one should expect an intermittent behavior, while for $R>W$ the dynamics of the orbit will be essentially diffusive, since the noise fluctuations are sufficient to drive the orbit always out of the SM valley. These indications suggest that in order to observe a "nontransient" or "nonintermittent" LFF dynamics the amount of noise present in the system should be larger than W. Also in [14] it has been clearly stated that the LK equations with parameters tuned to reproduce the dynamics of a DFB laser with $\alpha=3.4$ can give rise to stationary LFF's only in presence of noise.

It is important to remark that for $\alpha=3.3$ the experimentally measured variance of the noise $R=2.76\times10^{-3}$ is above the barrier $W=1.87\times10^{-3}$ found from the fit of the numerical $\langle T_{res} \rangle$ with expression (9), performed in the low-noise range (see Fig. 8). Moreover, in the experiments we never observed relaxation of the dynamics towards a SM.

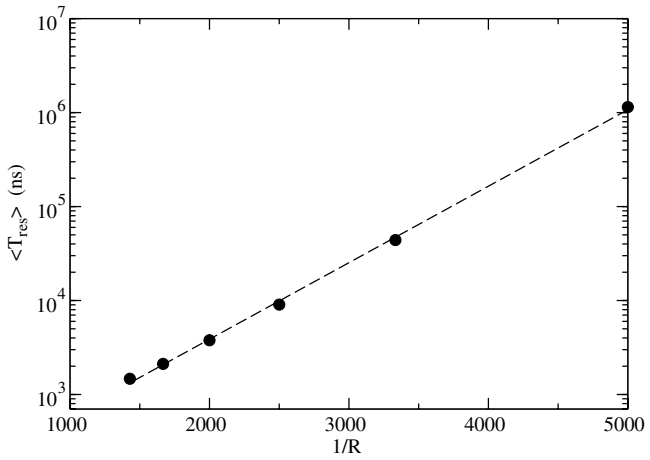

FIG. 8. Average residence times in the SM as a function of the inverse of the variance of the additive noise to the LK equations. The dashed line is a exponential fit $\propto \exp[W/R]$ to the numerical data; the fitted exponential slope is $W=0.00187$. The data refer to $\mu=0.97$ and $\alpha=3.3$.

Lyapunov analysis

Also in the noisy case we have examined the degree of chaoticity in the system by estimating the maximal Lyapunov exponent along noisy orbits of the system. The role of noise is fundamental in destabilizing the dynamics of the system and in rendering the asymptotic dynamics chaotic.

In particular, as shown in Fig. 9(a) we observe that at $\mu=0.93$ and $k=0.25$ the deterministic dynamics ($R=0$) is asymptotically stable in the range $\alpha \leqslant 4.4$, while the noisy dynamics becomes more and more chaotic for increasing R. For the value $R=3.3\times10^{-3}$, close to the experimental one, the dynamics is completely destabilized in the whole examined range $2.5 \leqslant \alpha \leqslant 4.5$, while for smaller R values the range of destabilization is reduced. These results confirm the role of noise in rendering the LFF an asymptotic phenomenon. Moreover, the maximal Lyapunov increases steadily with α at $R=3.3\times10^{-3}$. Similar findings apply in the case $\mu=0.97$ [see Fig. 9(b)].

The wild oscillations in the $\langle\lambda_1\rangle$ values observable at the level of noise $R<10^{-4}$ reflect the stability properties of the SM's attracting the asymptotic dynamics.

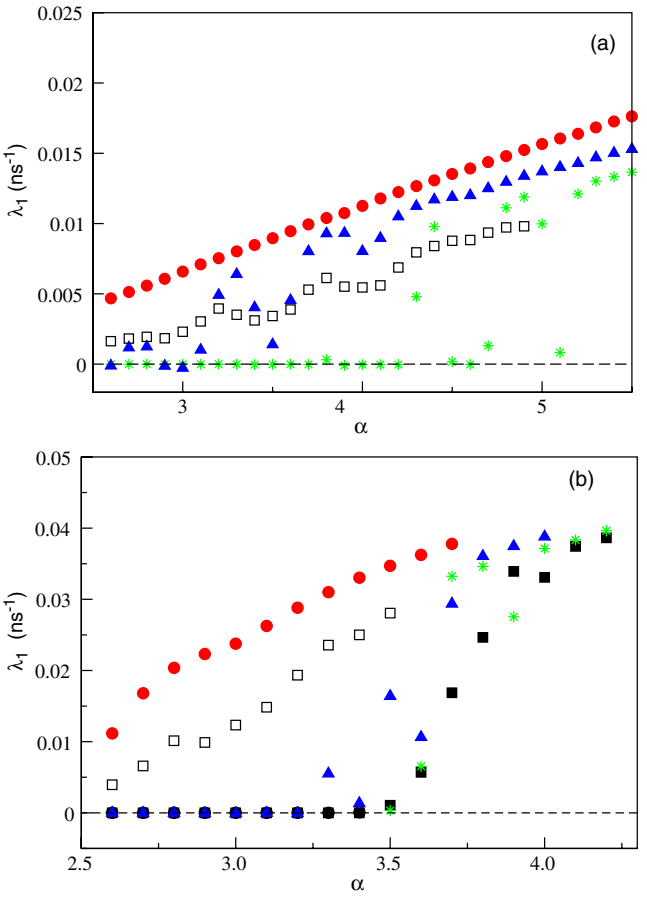

FIG. 9. (Color online) Maximal Lyapunov exponents λ_1 as a function of α for $\mu=0.93$ (a) and $\mu=0.97$ (b) and for various noise amplitudes R: namely, the data for $R=3\times10^{-5}$ are indicated by green asterisks, those for $R=3\times10^{-4}$ by blue solid triangles, and the ones corresponding to $R=3\times10^{-3}$ by red solid circles. The values estimated during the transient dynamics in the absence of noise are indicated by black open squares, while the asymptotic values for $R=0$ by black solid squares. All the data refer to $k=0.25$; for the estimation of λ_1 in the noisy case one orbit has been followed for a time $t=3.63$ ms with time step $\Delta t=0.363$ ps, while in the deterministic case the asymptotic results have also been averaged over $M=10$ different initial conditions. For details of the estimation of the transient Lyapunov exponents see the previous section V B.

VII. COMPARISON BETWEEN EXPERIMENTAL AND NUMERICAL DATA

This section will be devoted to a detailed comparison of numerical versus experimental results with the aim to clarify if the deterministic or noisy LK equations are indeed able to reproduce the experimental findings.

A. Distributions of the field intensities

As a first indicator we have considered the distribution of the field intensities $P(\rho^2)$; in particular, in order to match the experimental findings we consider a signal filtered at 200 MHz. A similar analysis has been reported in [44] for a semiconductor laser in the coherence collapse regime (i.e., for $I \gg I_{th}$).

The experimental results for the probability distribution functions (PDF's) of the field intensities ρ^2 are reported in Fig. 10 for various currents below the solitary threshold value. It should be noticed that the amplitudes ρ^2 have been rescaled in order to match the corresponding numerical values for the noisy LK equations with $\alpha=3.3$ and noise variance $R=3.3\times10^{-3}$, but that no arbitrarily shift has been applied to the data.

A peculiar characteristic of these data is that for increasing pump current the PDF's become more and more asymmetric, revealing a peak at large intensities that shifts to-

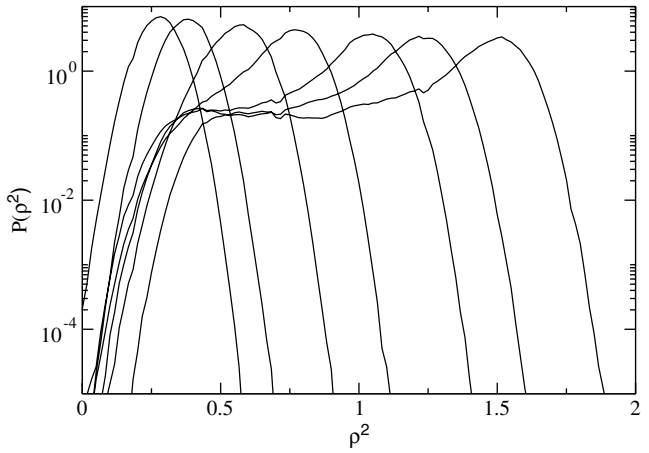

FIG. 10. Field intensities distributions $P(\rho^2)$ for the experimental signal filtered at 200 MHz. The experimental intensities have been arbitrarily rescaled to match the corresponding average intensities obtained from the simulation of the noisy LK equations at $\alpha=3.3$ and $k=0.35$ with noise variance $R=3.3\times10^{-3}$. The data refer from left to right to $I=2.48$ mA, 2.50, 2.54, 2.58, 2.64, 2.70, and 2.75. Since $I_{th}=2.76$, these data correspond to $0.9<\mu<1.0$. The first distribution has a large contribution from the Gaussian electronic noise, which also explains the negative ρ^2 values.

wards higher and higher ρ^2 values and a sort of plateau at smaller intensities.

The corresponding PDF's are reported in Figs. 11 and 12 for data obtained from the integration of the noisy and deterministic LK equations, respectively. Better agreement between numerical and experimental findings is found for the noisy dynamics with $\alpha\sim3.3$–4.0 and $k=0.35$, with a noise variance similar to the experimental one (namely, $R=3\times10^{-3}$). For the deterministic case (reported in Fig. 12 for $\alpha=5.0$ and $k=0.35$) a nonzero tail at $\rho\sim0$ is observed even for $\mu\sim1.0$, contrary to what is observed for the experimental data.

These results indicate that it is necessary to include the noise in the LK equation to obtain a reasonable agreement with the experiment, at least at the level of the intensity PDF's. However, the numerical data seem unable to reproduce the narrow peak present in the experimental ones at large intensities and for $\mu\rightarrow1$. In the next subsection a further comparison will be performed to validate these preliminary indications.

B. Average values of the LFF times

We will first compare the experimental and numerical measurements of the average times between two consecutive drops of the field intensities, $\langle T_{LFF}\rangle$. They have been evaluated in two (consistent) ways: from a direct measurement of periods between threshold crossing and from the Fourier power spectrum of the temporal signal $\rho^2(t)$.

Direct measurements of the T_{LFF} from the time trace of $\rho^2(t)$ have been performed by defining two thresholds $\Gamma_1<\Gamma_2$ and by identifying two consecutive time crossings of Γ_1, provided that in the intermediate time the signal has overcome the threshold Γ_2 at least once. The thresholds have been defined as $\Gamma_1=\langle\rho^2\rangle-2\mathcal{S}$ and $\Gamma_2=\langle\rho^2\rangle+\mathcal{S}/2$, where $\langle\cdot\rangle$ and $\mathcal{S}$ indicate the average and standard deviations of the signal itself.

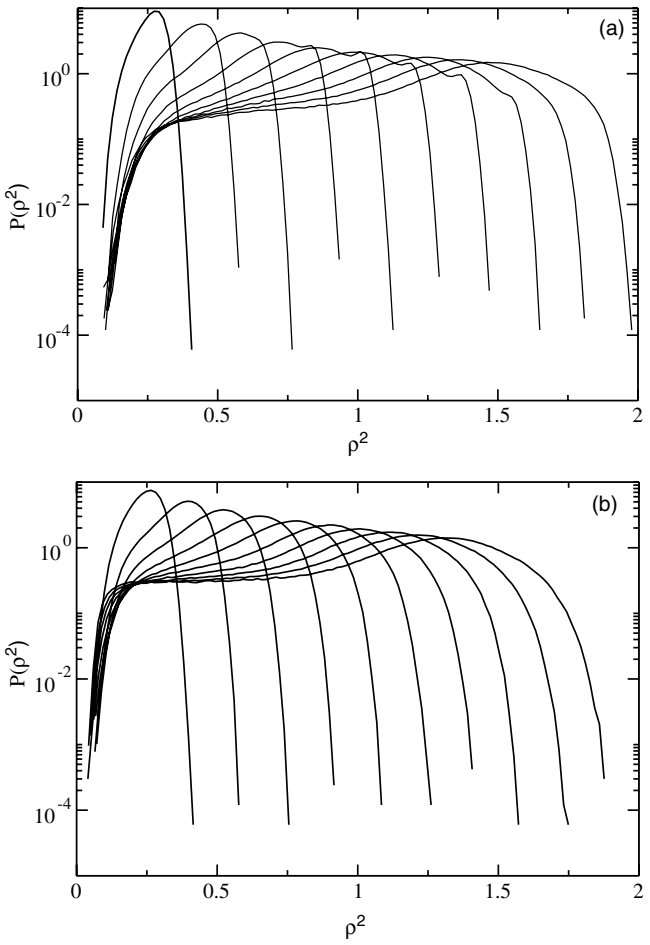

FIG. 11. Field intensity distributions $P(\rho^2)$ for the numerical data obtained by the integration of a noisy LK equations filtered at 200 MHz. The data refer from left to right to $\mu=0.90$, 0.91, 0.92, 0.93, 0.94, 0.95, 0.96, 0.97, 0.98, and 0.99 for (a) $\alpha=3.3$ and (b) $\alpha=4.0$. Both the sets of data correspond to $k=0.35$ and noise variance $R=3\times10^{-3}$.

The measurement of $\langle T_{LFF}\rangle$ in terms of the power spectrum has been obtained by considering the power spectrum $S(\omega)$ of $\rho^2(t)$ and by evaluating the position ω_M of the peak with the highest frequency; then, $\langle T_{LFF}\rangle=2\pi/\omega_M$. As already mentioned the two estimations are generally in very good agreement.

In Fig. 13 the average times $\langle T_{LFF}\rangle$ are reported for two different sets of experimental measurements as a function of the pump parameter μ and compared with numerical data. In Fig. 13(a) are reported the experimental findings already shown in [15]; the estimation of T_{LFF} has been performed both by direct inspection of the signal and via the first zero of the autocorrelation function (this second method corresponds to an evaluation from the Fourier power spectrum). The numerical data have been obtained with the two methods outlined above for $k=0.25$ for both noisy and deterministic LK equations In Fig. 13(b) a new set of experimental data is reported and compared with simulation results for $k=0.35$; in

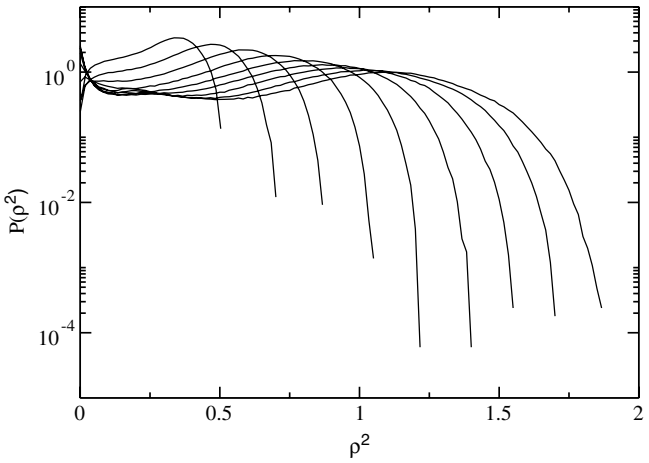

FIG. 12. Field intensity distributions $P(\rho^2)$ for the numerical data obtained by the integration of a deterministic LK equations filtered at 200 MHz. The data refer from left to right to μ=0.91, 0.92, 0.93, 0.94, 0.95, 0.96, 0.97, 0.98, and 0.99 for α=5.0 and k =0.35.

this case, all the data have been obtained by the method of thresholds. From the figures it is clear that reasonably good agreement between experimental and numerical data is observed for the deterministic case only for α=5 (results for smaller α values, obtained during the transient preceding the stable phase, are not shown but they exhibit a worse agreement with experimental findings) and for the noisy dynamics for α=4.0.

A more detailed analysis can be obtained by considering not only the average values of the LFF times, but also the associated standard deviation V. This quantity, reported in Fig. 14, exhibits a clear decrease with μ by approaching the solitary threshold, indicating a modification of the observed dynamics that tends to be more "regular." Also in this case comparison of experimental and numerical data suggests that the best agreement is again attained with the noisy dynamics at α=4.0.

At this stage of the comparison we can sketch some preliminary conclusions: the LK equations are able to reproduce reasonably well the experimental data for the VCSEL below the solitary threshold both in the deterministic case and in the noisy situation. However, in the deterministic case a quite large value of the linewidth enhancement factor (with respect to the experimentally measured one) is required. A more detailed comparison will be possible by considering the PDF's of the T_{LFF}.

C. Distributions of the LFF times

In this subsection we will examine the whole distribution of the T_{LFF} in more detail. Considering the experimental data, we observe that all the measured PDF's obtained for different pump currents reveal an exponential-like tail at long times and a rapid drop at short times (as shown in Fig. 15). These results are in agreement with those reported in [18] for a single-transverse-mode semiconductor laser in proximity of I_{th}.

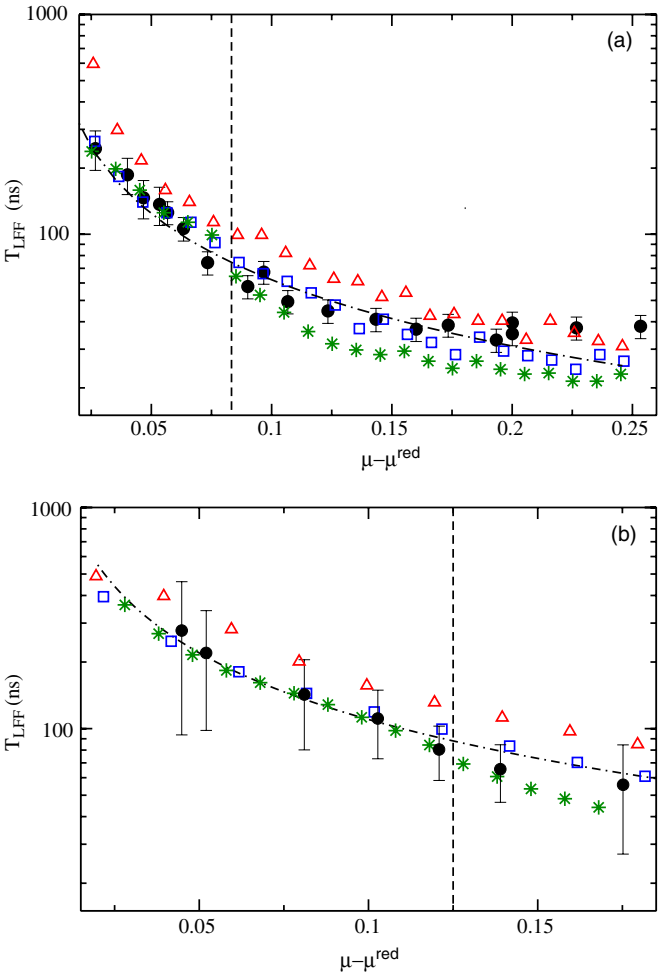

FIG. 13. (Color online) Average LFF times $\langle T_{LFF}\rangle$ as a function of the pump parameter $\mu-\mu^{red}$: black solid circles refer to experimental data, while the other symbols to the results obtained from the integration of the LK equations. In the two figures are reported two different sets of experimental measures and the associated numerical data refer to k=0.25 (a) and k=0.35 (b). In particular, red open triangles correspond to the evolution of the noisy LK model at α=3.3 [with (a) μ^{red}=0.914 and (b) μ^{red}=0.880] and blue open squares to α=4.0 [with μ^{red}=0.913 and 0.878 for (a) and (b) respectively]. In both cases $R=3\times10^{-3}$. The green stars denote the data of the deterministic LK equations for α=5.0 [in this case μ^{red}=0.915 and 0.882 for (a) and (b), respectively]. For the experimental measures μ^{red}=0.916 in (a) and 0.875 in (b). The vertical dashed lines indicate the position of the solitary threshold for the experimental data, while the dash-dotted lines represent the decay $c/(\mu-\mu^{red})$, with c=6.2 ns and 11 ns in (a) and (b), respectively. μ^{red} is defined as the ratio I_{th}^{red}/I_{th}.

The typical dynamics corresponding to a LFF can be summarized as follows: a sudden drop of intensity is followed by a steady increase of ρ^2, associated with fluctuations of the intensity, until a certain threshold is reached and the intensity is reset to its initial value and restarted with the same "Sisyphus cycle" [5]. This behavior and the observed shapes of the PDF's suggest that the dynamics of the intensities can be modeled in terms of a Brownian motion plus drift. In other words, by denoting by $x(t)$ the intensity, an effective equa-

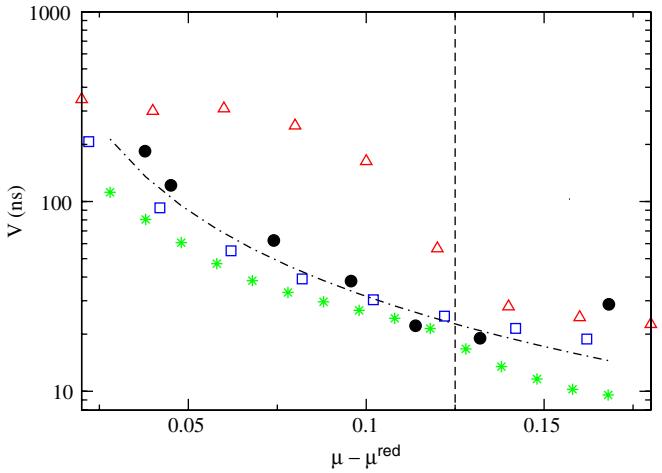

FIG. 14. (Color online) Standard deviation of the LFF times V as a function of the pump parameter $\mu-\mu^{red}$: the symbols are the same as those reported in Fig. 13(b). The dash-dotted line indicates the power-law decay $1/(\mu-\mu^{red})^{3/2}$.

tion of the following type can be written to reproduce its dynamical behavior:

$$\dot{x}(t) = \eta + \sigma\xi(t), \tag{10}$$

with initial condition $x(0)=x_0$, where $\xi(t)$ is a Gaussian noise term with zero average and unitary variance, η represents the drift, and σ is the noise strength. Within this framework the average first-passage time to reach a fixed threshold Γ is simply given by $\tau=(\Gamma-x_0)/\eta$, while the corresponding standard deviation is $V=[\sqrt{(\Gamma-x_0)}\sigma]/\eta^{3/2}$ [42]. A reasonable assumption would be that η is directly proportional to the pump parameter $(\mu-\mu^{red})$, (where $\mu^{red}=I_{th}^{red}/I_{th}$ is the rescaled pump current value at the reduced threshold) and by further assuming that the threshold Γ is independent of the pump current this would imply that

$$\langle T_{LFF}\rangle = \frac{c}{(\mu-\mu^{red})}, \quad V_{LFF} = \frac{c}{(\mu-\mu^{red})^{3/2}}. \tag{11}$$

These dependences are indeed quite well verified for experimental data above the solitary threshold as shown in Figs. 13 and 14.

For the simple model introduced by Eq. (10), the PDF of the first-passage times is the so-called inverse Gaussian distribution [43]

$$P(T) = \frac{\tau}{\sqrt{2\pi\gamma T^3}} e^{-(T-\tau)^2/(2\gamma T)}, \tag{12}$$

where $\gamma=V^2/\tau$. A comparison of this expression with the experimentally measured $P(T_{LFF})$ is reported in Fig. 15. The good agreement suggests that the "Sisyphus cycles" can be due to a few elementary ingredients: a stochastic motion subjected to a drift plus a reset mechanism once the intensity has overcome a certain threshold.

A way of rewriting the distribution (12) in a more compact form as a function of only one parameter, the so-called coefficient of variation $\delta=V/\tau$ (i.e., the ratio between the standard deviation V and the mean τ), is to rescale the time as $z=(T-\tau)/V$ and the PDF's as $g(z)=VP(T)$. This procedure leads to the following expression:

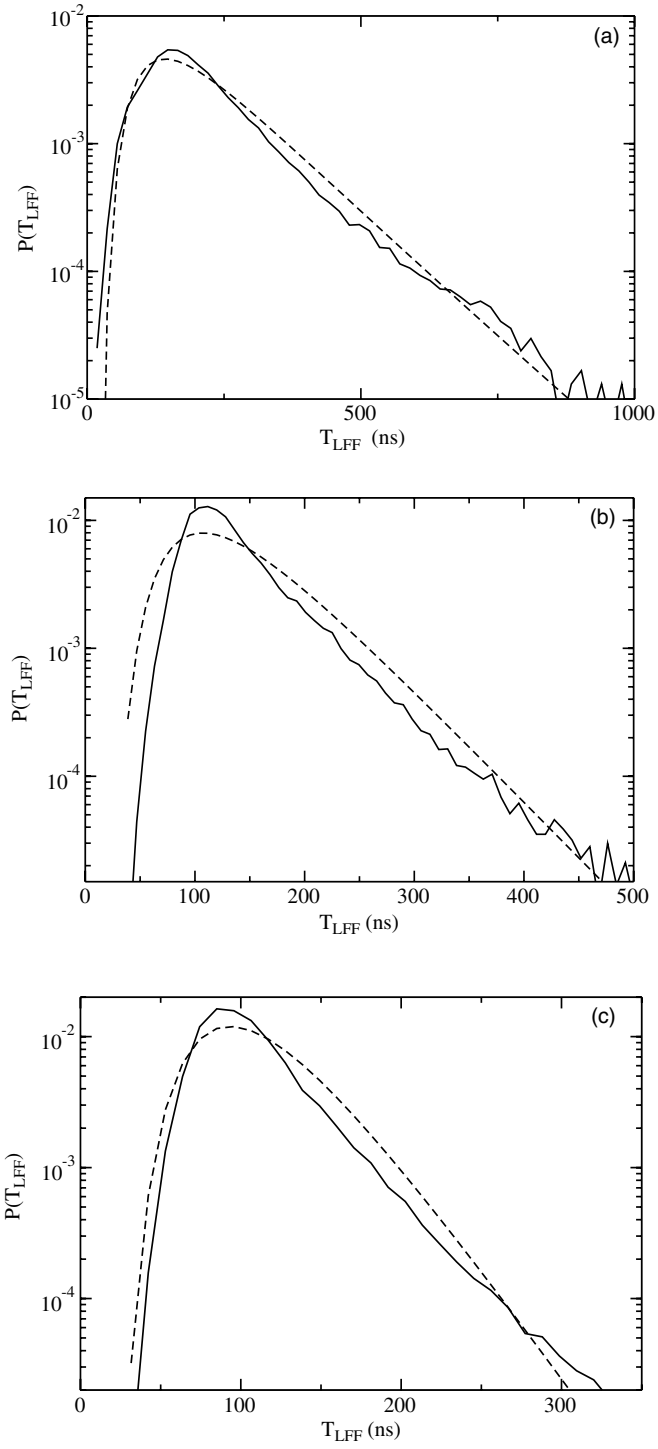

FIG. 15. Probability density distributions of the T_{LFF}. Solid lines refer to experimental data, the dashed ones to the inverse Gaussian distribution (12) with the average and standard deviations corresponding to the experimental ones. (a) $I=2.56$ mA, (b) $I=2.64$ mA, and (c) $I=2.70$ mA.

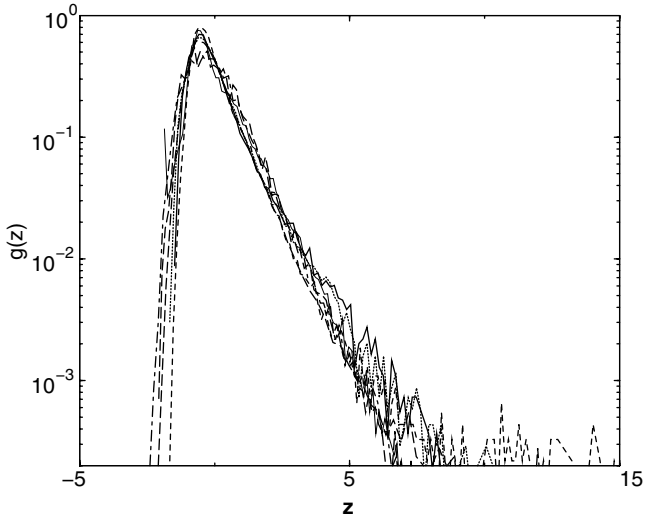

FIG. 16. Rescaled probability density distributions $g(z)=VP(T_{LFF})$ as a function of $z=(T_{LFF}-\langle T_{LFF}\rangle)/V$. The curves refer to $I=2.54$ mA, 2.56 mA, 2.64 mA, 2.70 mA, 2.75 mA, 2.80 mA, and 2.90 mA.

$$g(z)=\frac{1}{\sqrt{2\pi(\delta z+1)^3}}e^{-z^2/2(\delta z+1)}. \tag{13}$$

It is clear that all PDF's will coincide, once rescaled in this way, if the coefficient of variation, δ, has the same value for all considered pump currents. However, this is not the case and indeed we measured values of δ in the range $[0.28, 0.66]$ for $I<I_{th}$; nonetheless, if we report in a single graph all these curves, the overall matching is very good, as shown in Fig. 16.

Let us finally compare these distributions $g(z)$ with the corresponding ones obtained from direct simulations of the LK equations. As one can see from Fig. 17 the agreement is good for the data obtained from the simulation of the noisy LK equations at $\alpha=4.0$, while it is worse for the deterministic LK equations at $\alpha=5.0$.

VIII. CONCLUSIONS

We presented a detailed experimental and numerical study of a semiconductor laser with optical feedback. The choice of a vertical cavity laser pumped close to its threshold, together with a polarized optical feedback, assures great control over the possibility of lasing action of other order longitudinal and/or transverse modes than the fundamental one and of the activation of the other polarization. In such a way, the description of the system using the Lang-Kobayashi model is well justified and it allows for a meaningful comparison with the experimental data. The analysis has been performed with particular regard to the LFF regime, where the model has been numerically integrated using parameters carefully measured in the laser sample used for the measurements.

The comparison of the measurements carried out in the VCSEL with polarized optical feedback with the predictions of the deterministic LK model suggests that in the examined

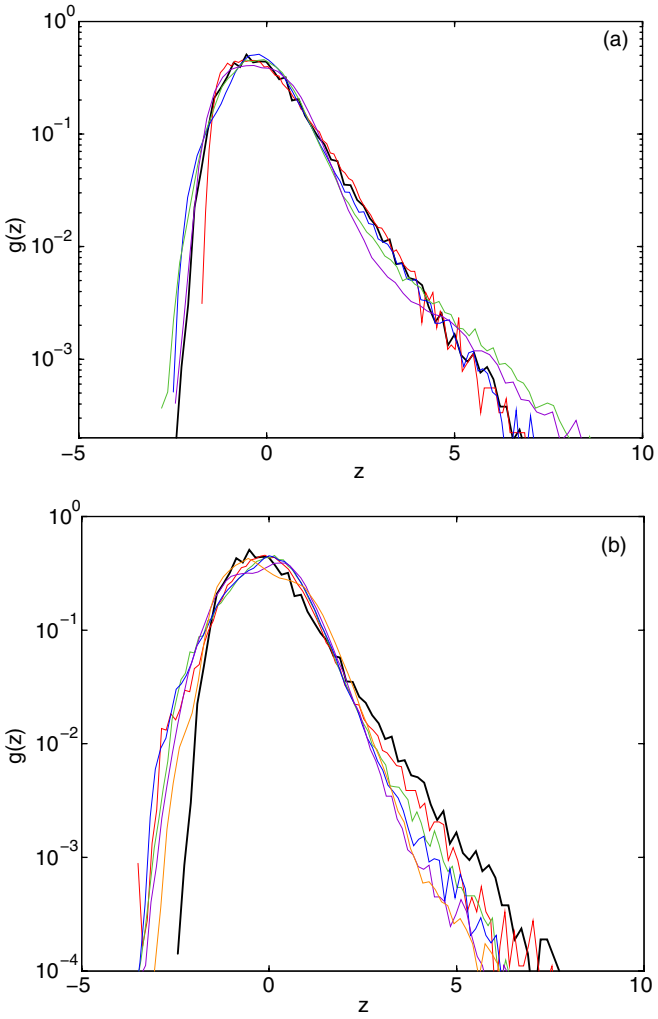

FIG. 17. (Color online) Rescaled probability density distributions $g(z)=VP(T_{LFF})$ as a function of $z=(T_{LFF}-\langle T_{LFF}\rangle)/V$. The thick solid curve refers to experimental data for $I=2.75$ mA (corresponding to $\mu\simeq 1$), the other ones to numerical findings: (a) data obtained for the noisy LK equations for $\alpha=4.0$, $k=0.35$ with variance $R=3\times10^{-3}$ and corresponding to $\mu=0.90$ (red), 0.94 (blue), 0.98 (green), and 1.02 (violet); (b) data for the deterministic LK equations for $\alpha=5.0$, $k=0.35$ corresponding to $\mu=0.92$ (red), 0.94 (blue), 0.96 (green), 0.98 (violet), and 1.00 (orange).

range of parameters the dynamics of the model is characterized by a chaotic transient leading to stable ECM's with high gain. The transient duration increases (and possibly diverges) with increasing values of the rescaled pump current μ and of the linewidth enhancement factor α. We have not found evidence of periodic or quasiperiodic asymptotic attractors; as instead reported in [6], this can be due to the α range examined in the present paper (namely, $2.4\leqslant\alpha\leqslant5.5$), since these solutions become relevant for the dynamics only for $\alpha>5$ (as stated in [6]).

However, a stationary LFF dynamics with characteristics similar to those measured experimentally can be obtained for realistic values of the α parameter (namely, $\alpha\sim3-4$) only via the introduction of an additive noise term in the LK equations. The role of noise in determining the statistics and the nature of the dropout events has been previously exam-

ined in [3,4], but in the present paper we have clarified that the LFF dynamics can be interpreted at a first level of approximation as a biased Brownian motion towards a threshold with a reset mechanism.

Finally, a detailed analysis of the experimental and numerical data indicates that while the statistics of the experimental LFF times can be quantitatively well reproduced by the simulations, the agreement between the experimental and simulated field intensities distributions is definitely satisfactory at a qualitative level, but not yet quantitatively.

ACKNOWLEDGMENTS

We acknowledge useful discussions with M. Bär, S. Yanchuk, S. Lepri, and M. Wolfrum. Two of us (G.G. and F.M.) thank C. Piovesan for his effective support.

[1] C. Risch and C. Voumard, J. Appl. Phys. **48**, 2083 (1977).
[2] *Fundamental Issues of Nonlinear Laser Dynamics*, AIP Conf. Proc. No. 548, edited by B. Krauskopf and D. Lenstra (AIP, Melville, NY, 2000).
[3] C. H. Henry and R. F. Kazarinov, IEEE J. Quantum Electron. **QE-22**, 294 (1986).
[4] A. Hohl, H. J. C. van der Linden, and R. Roy, Opt. Lett. **20**, 2396 (1995).
[5] T. Sano, Phys. Rev. A **50**, 2719 (1994).
[6] R. L. Davidchack, Y.-C. Lai, A. Gavrielides, and V. Kovanis, Phys. Rev. E **63**, 056206 (2001).
[7] T. W. Carr, D. Pieroux, and P. Mandel, Phys. Rev. A **63**, 033817 (2001).
[8] I. Pierce, P. Rees, and P. S. Spencer, Phys. Rev. A **61**, 053801 (2000).
[9] E. A. Viktorov and P. Mandel, Phys. Rev. Lett. **85**, 3157 (2000).
[10] G. Huyet, S. Balle, M. Giudici, C. Green, G. Giacomelli, and J. R. Tredicce, Opt. Commun. **149**, 341 (1998).
[11] G. Vaschenko, M. Giudici, J. J. Rocca, C. S. Menoni, J. R. Tredicce, and S. Balle, Phys. Rev. Lett. **81**, 5536 (1998).
[12] A. A. Duarte and H. G. Solari, Phys. Rev. A **64**, 033803 (2001); **60**, 2403 (1999); **58**, 614 (1998).
[13] M. Giudici, C. Green, G. Giacomelli, U. Nespolo, and J. R. Tredicce, Phys. Rev. E **55**, 6414 (1997).
[14] T. Heil, I. Fischer, W. Elsässer, J. Mulet, and C. R. Mirasso, Opt. Lett. **24**, 1275 (1999).
[15] G. Giacomelli, F. Marin, and M. Romanelli, Phys. Rev. A **67**, 053809 (2003).
[16] G. Vaschenko, M. Giudici, J. J. Rocca, C. S. Menoni, J. R. Tredicce, and S. Balle, Phys. Rev. Lett. **81**, 5536 (1998).
[17] D. W. Sukow, T. Heil, I. Fischer, A. Gavrielides, A. Hohl-AbiChedid, and W. Elsässer, Phys. Rev. A **60**, 667 (1999).
[18] D. W. Sukow, J. R. Gardner, and D. J. Gauthier, Phys. Rev. A **56**, R3370 (1997).
[19] J. Mulet and C. R. Mirasso, Phys. Rev. E **59**, 5400 (1999).
[20] W.-S. Lam, W. Ray, P. N. Guzdar, and R. Roy, Phys. Rev. Lett. **94**, 010602 (2005).
[21] R. Lang and K. Kobayashi, IEEE J. Quantum Electron. **16**, 347 (1980).
[22] F. Rogister, M. Sciamanna, O. Deparis, P. Mégret, and M. Blondel, Phys. Rev. A **65**, 015602 (2001).
[23] M. Giudici, S. Balle, T. Ackemann, S. Barland, and J. Tredicce, J. Opt. Soc. Am. B **16**, 2114 (1999).
[24] T. E. Sale, *Vertical Cavity Surface Emitting Lasers* (Wiley, New York, 1995).
[25] A. V. Naumenko, N. A. Loiko, M. Sondermann, and T. Ackemann, Phys. Rev. A **68**, 033805 (2003).
[26] C. Masoller and N. B. Abraham, Phys. Rev. A **59**, 3021 (1999).
[27] N. A. Loiko, A. V. Naumenko, and N. B. Abraham, Quantum Semiclassic. Opt. **10**, 125 (1998).
[28] N. A. Loiko, A. V. Naumenko, and N. B. Abraham, J. Opt. B: Quantum Semiclassical Opt. **3**, S100 (2001).
[29] P. Besnard, F. Robert, M. L. Charés, and G. M. Stéphan, Phys. Rev. A **56**, 3191 (1997).
[30] K. H. Gulden, M. Moser, S. Lüscher, and H. P. Schweizer, Electron. Lett. **31**, 2176 (1995).
[31] M. C. Soriano, M. Yousefi, J. Danckaert, S. Barland, M. Romanelli, G. Giacomelli, and F. Marin, IEEE J. Sel. Top. Quantum Electron. **10**, 998 (2004).
[32] S. Barland, P. Spinicelli, G. Giacomelli, and F. Marin, IEEE J. Quantum Electron. **41**, 1235 (2005).
[33] J. D. Farmer, Physica D **4**, 366 (1982).
[34] M. San Miguel and R. Toral, in *Instabilities and Nonequilibrium Structures* VI, edited by E. Tirapegui and W. Zeller (Kluwer Academic, Dordrecht, 1997).
[35] I. Shimada and T. Nagashima, Prog. Theor. Phys. **61**, 1605 (1979); G. Benettin, L. Galgani, A. Giorgilli and J. M. Strelcyn, Meccanica, No. 3, 21 (1980).
[36] J. L. Kaplan and J. A. Yorke, Lect. Notes Math. **13**, 730 (1979).
[37] S. Yanchuk and M. Wolfum (unpublished).
[38] S. Yanchuk and M. Wolfrum, in *Proceedings of the Fifth EUROMECH Nonlinear Dynamics Conference (ENOC-2005), Eindhoven, Netherlands, 2005*, edited by D. H. van Campen, M. D. Lazurko, and W. P. J. M. van der Oever (Eindhoven University of Technology, Eindhoven, 2005) pp. 1060–1065.
[39] A. M. Levine, G. H. M. van Tartwijk, D. Lenstra, and T. Erneux, Phys. Rev. A **52**, R3436 (1995).
[40] J. M. Méndez, J. Aliaga, and G. B. Mindlin, Phys. Rev. E **71**, 026231 (2005).
[41] T. Heil, I. Fischer, and W. Elsässer, Phys. Rev. A **58**, R2672 (1998).
[42] H. C. Tuckwell, *Introduction to Theoretical Neurobiology* (Cambridge University Press, Cambridge, England, 1988).
[43] R. S. Chikara and J. L. Folks, *The Inverse Gaussian Distribution* (Marcel Dekker, New York, 1988).
[44] G. Huyet, S. Hegarty, M. Giudici, B. de Bruyn, and J. G. McInerney, Europhys. Lett. **40**, 619 (1997).
[45] For $\mu=0.97$ a variation of α from 3.48 to 3.60 leads to an increase of $\langle T_s \rangle$ from 130 μs to 1.3 ms.